Acta Crystallographica Section A
Foundations of Crystallography
ISSN 0108-7673

Received 24 July 2006
Accepted 8 November 2006

Accurate structure factors and experimental charge densities from synchrotron X-ray powder diffraction data at SPring-8

Eiji Nishibori,[a]* Eiji Sunaoshi,[a] Akihiro Yoshida,[a] Shinobu Aoyagi,[a] Kenichi Kato,[b,c,d] Masaki Takata[b,c,d] and Makoto Sakata[a]

[a]Department of Applied Physics, Nagoya University, Nagoya 464-8603, Japan, [b]Japan Synchrotron Radiation Research Institute, 1-1-1 Kouto, Sayo-cho, Sayo-gun, Hyogo 679-5198, Japan, [c]CREST, JST, Japan, and [d]Structural Materials Science Laboratory, RIKEN SPring-8 Center, 1-1-1 Kouto, Sayo-cho, Sayo-gun, Hyogo 679-5148, Japan. Correspondence e-mail: eiji@mcr.nuap.nagoya-u.ac.jp

Accurate structure factors of silicon and diamond have been experimentally determined from powder diffraction data measured at the third-generation synchrotron-radiation source SPring-8, BL02B2. The accuracy of the obtained structure factors has been evaluated by comparing with structure factors in the literature measured by the *Pendellösung* method and with some from theoretical calculations. The results indicate that the structure factors from powder data are accurate enough to discuss the experimental charge-density distributions of these materials. The number of structure factors of silicon determined in the present study is 104, which is three times more than that of previous *Pendellösung* data. The experimental charge densities have been obtained by the maximum-entropy method from the present structure factors. The charge densities at bond mid-points for silicon and diamond show good agreement with different kinds of theoretical calculations. The present study proved that the powder diffraction at SPring-8 is a promising method for determination of experimental charge density for a wider range of materials.

1. Introduction

The electron-density distribution in materials determines their properties and functions. For example, the hardness of diamond is due to the strong three-dimensional covalent-bond network formed by the valence electrons of C atoms. Many attempts in both experimental and theoretical researches in materials science such as diffraction, spectroscopic studies and density functional calculations (DFT) have been performed to reveal the electron-density distributions in many materials. The information of electron distributions in materials gives a clue to the development and the design of new functional materials.

An X-ray is a very good probe of electrons. The structure factors from X-ray diffraction give information on the total electron-density distribution including both the core and the valence electrons. Accurate structure factors are always required in materials science fields, since the structure factors can be used not only for experimental charge-density studies but also for the evaluation of different theoretical calculations. The required accuracy of structure factors for these purposes is much higher than that of a normal crystallographic structural study at atomic level, where the main concern is the atomic arrangement only.

Structure factors can be measured by various methods, such as the *Pendellösung* fringe method, single-crystal diffraction and powder diffraction. The *Pendellösung* method is feasible for structure-factor determination with enough accuracy, claimed better than 0.5%, which must be a great advantage for charge-density study. The disadvantage of the method lies in the need for a large perfect crystal of well defined wedge shape. Therefore, target materials have been extremely limited such as silicon (Saka & Kato, 1986) and diamond (Takama *et al.*, 1990). Single-crystal diffraction, which does not require a perfect crystal, is very commonly used. The disadvantage of the method for determining accurate charge densities is that it needs extinction correction for low-order reflections, which carries important information on chemical bonding. Accurate charge-density studies from single-crystal diffraction have been commonly performed particularly for organic and metal-organic compounds, where the extinction is relatively small.

In the case of powder diffraction, the range of target materials is extensively broader than those of the *Pendellösung* method and single-crystal diffraction. However, the accuracy of powder diffraction data has been considered to be much poorer than that of the *Pendellösung* method and the single-crystal diffraction method due to the following reasons.

Firstly, the measured integrated Bragg intensities are relatively weak. Secondly, it is difficult to obtain the individual integrated Bragg intensities due to peak overlaps and other relatively minor reasons. Therefore, it has been considered that powder diffraction data are not appropriate for accurate charge-density studies.

Recent progress in the synchrotron powder X-ray diffraction technique including the third-generation synchrotron X-ray source, detector, measurement system and analytical method provides us with a possibility to obtain accurate structure factors for charge-density studies. Powder data with high intensity and high angular resolution have now become available. We have installed a large Debye–Scherrer camera for accurate charge-density studies at SPring-8, BL02B2. Detailed specification of this camera and its performance has been described elsewhere (Nishibori, Takata, Kato *et al.*, 2001). The precise charge densities of $PbTiO_3$ (Kuroiwa *et al.*, 2001), fullerene-related materials (Nishibori, Takata, Sakata, Taninaka & Shinohara, 2001) and the MgB_2 superconductor (Nishibori, Takata, Sakata, Tanaka, Muranaka & Akimitsu, 2001) have been determined from powder diffraction data measured by the camera. For proper understanding of the charge densities determined by SPring-8 powder data, quantitative estimation of the accuracy of the data is essential. Evaluation of the quantitative accuracy of diffraction data is not an easy task. Benchmark tests need accurate data from both experiment and theoretical sides.

There are accurate structure factors of silicon and diamond measured by various experimental methods, such as the *Pendellösung* method (Saka & Kato, 1986; Takama *et al.*, 1990) and the fine oscillatory structure of Laue-case rocking curves (Teworte & Bonse, 1984). These data have been widely used for experimental charge-density studies by the multipole refinement (Spackman, 1986, 1991) and by the maximum-entropy method (MEM) (Sakata & Sato, 1990; Takata & Sakata, 1996). Furthermore, the data have been widely used for evaluation of the performance of theoretical calculations, such as the several types of the linear augmented plane-wave method (LAPW) (Trail & Bird, 1999; Zuo *et al.*, 1997; Pere *et al.*, 1999), the linear combination of atomic orbitals Hartree–Fock method (LCAO–HF) (Zuo *et al.*, 1997; Pere *et al.*, 1999), and the multiconfigurational Dirac–Fock method (MCDF) (Zuo *et al.*, 1997). These data are used in the evaluation of the accuracy of the powder data measured at SPring-8, BL02B2.

In this study, we have measured accurate powder diffraction data of both silicon and diamond at SPring-8, BL02B2. Then we extracted structure factors from powder diffraction data. The accuracy of the data has been estimated by comparison with both the *Pendellösung* data and several theoretical calculations. Through such procedures, the accuracies of both structure factors and charge density from powder data at SPring-8 is fully discussed in the present study. Then the charge-density distributions of Si and diamond obtained by the MEM are shown in order to point out the usefulness of powder data for charge-density studies.

2. Synchrotron X-ray powder diffraction experiment

2.1. Sample preparations

Powder data for charge-density study must have homogeneous intensity distribution along Debye–Scherrer rings. Powder samples with grain sizes of a few μm are appropriate for obtaining this. A standard powder sample of silicon by the National Institute of Standards and Technology (NIST) was used in this study. The median particle size was 4.9 μm. A diamond powder by the Nilaco Corporation was also used as a sample. The average particle size was 6 μm. The powder samples were agglomerated together with a tiny amount of glue. The agglomerated samples were cut into a rectangle. By using this sample, we did not need to use a glass capillary in the experiment. This is to reduce background scattering in diffraction data. The sizes of the agglomerated rectangle samples are approximately $3.0 \times 0.3 \times 0.3$ mm.

2.2. X-ray diffraction experiment

The synchrotron powder diffraction experiments were carried out at SPring-8, BL02B2 beamline (Nishibori, Takata, Kato *et al.*, 2001). High-energy X-rays, 0.40122 (1) Å, were used for reducing the absorption effect. In the case of silicon, the angular variation of absorption between 0 and 80° at 2θ is less than 0.1%. 80° at 2θ is the maximum diffraction angle in the present study. In the case of diamond, the variation is less than 0.02%. Owing to the small effects, absorption correction is ignored in the present study. The sample was oscillated at the centre of the diffractometer during the exposure time to improve intensity homogeneity along the Debye–Scherrer ring. The beam size was 3 mm in width and 0.7 mm in height.

Powder data for accurate charge-density study require high counting statistics and high angular resolutions. The higher-angle reflections have a disadvantage when high counting statistics data are collected because of the Lorentz factor, the X-ray atomic scattering factor and the temperature factor. To improve counting statistics of data in the higher-angle range, we measured two data sets for each sample at each temperature point. One data set (D_1) was measured by the normal procedure including all the reflections. Another data set (D_2) was measured to improve the counting statistics of high-order reflections excluding low-order reflections, some of which are very strong. The exposure times of the data collection were estimated from the preliminary measurement with 5 min exposure for both silicon and diamond. The exposure time of D_1 was the time for the maximum intensity of the 111 reflection to become 80% of the detection limit for the Imaging Plate (IP). The exposure time of D_2 was more than four times longer than D_1. The D_1 and D_2 data collections were carried out successively and recorded on the same IP (200×400 mm) using slit with 10 mm width. The slit was placed in front of the IP cassette. The D_2 data were measured by moving the IP cassette in the direction of 2θ to avoid some very strong low-angle reflections. The experimental conditions between D_1 and D_2 were kept identical as much as possible.

The IP was read after 30 min from the end of X-ray exposure to avoid the fading effects of the IP (Amemiya, 1995).

One-dimensional powder diffraction data were obtained by an integration with 51 pixels, which corresponds to 0.25 mm ordinary slit height. For the integration of the X-ray powder diffraction data collected on the IP, there are several programs, such as *FIT2D* (Hammersley *et al.*, 1996). In this study, software with graphical IP viewer, which is called *IPV*, has been coded for changing two-dimensional IP data to one-dimensional powder data.

The intensity distributions along the Debye–Scherrer ring of 111 reflection is shown in Fig. 1 for both (*a*) silicon and (*b*) diamond. It shows that intensity distributions are very homogeneous. The fluctuation of intensity is less than 1%. Thus, it is concluded that these data are appropriate for accurate structural analysis.

2.3. Data quality and forbidden reflections

Diffraction data in both silicon and diamond show intensity for 'forbidden' reflections such as 222 due to covalent bonding electrons. The forbidden reflections are normally considered unmeasurable in powder diffraction owing to their very weak intensities. The intensity of forbidden reflections is less than 0.1% of that of 111 reflections. In this study, the 222 so-called forbidden reflections were measurable for both silicon and diamond. The peak profiles of 222 reflections of silicon and diamond are shown in Figs. 2(*a*) and (*b*), respectively. There is no technical problem in calculating Bragg integrated intensities from Fig. 2. The intensity ratios between 222 and 111 were very small, *i.e.* 0.01% in silicon and 0.1% in diamond. This fact indicates that detection limit of powder data at SPring-8 BL02B2 is better than 0.01%.

3. Data analysis

To extract accurate structure factors from two powder data sets with different statistics and angular ranges, simultaneous analysis of two data sets is most suitable. In the profile analysis including weak forbidden reflections, a careful treatment of the tail of the powder profiles is required. The 222 reflection is overlapping on the tail of the 311 reflection as shown in Fig. 2(*a*). It was found that a split-type pseudo-Voigt function was the most suitable to fit the tail of the 311 reflection after several trials. There is much software, such as *GSAS* (Larson & Von Dreele, 1990) and *Fullprof* (Roisnel & Rodriguez-Carvajal, 2001), for powder data analysis. However, these programs have some insufficient areas for the present purpose, *i.e.* precise analysis of the present SPring-8 powder data. For example, an appropriate way to treat multi-synchrotron data sets is not known and also how background scattering can be subtracted for very weak reflections. Powder patterns collected at SPring-8 have several special features, which have

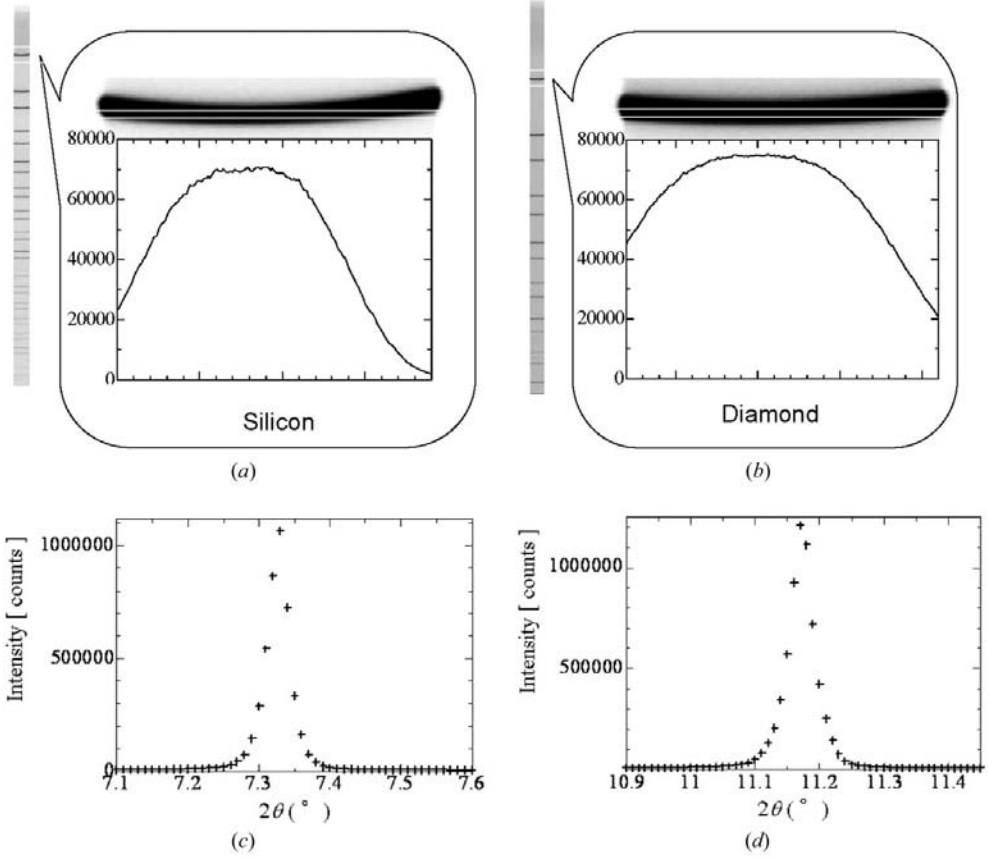

Figure 1
The intensity distributions on 111 Debye–Scherrer ring for (*a*) silicon and (*b*) diamond. Powder profiles of 111 reflections for (*c*) silicon and (*d*) diamond are also shown.

never been encountered by any other powder diffraction experiment, such as a wide dynamic range and very high resolution. Thus, we developed Rietveld refinement software, which is suitable for accurate structural analysis of SPring-8 powder data. Some features of the developed software called synchrotron-powder (SP) are as follows: (i) it allows simultaneous refinement of two different sets of powder diffraction data at SPring-8, BL02B2; (ii) it allows us to choose one of several types of split-type profile functions, such as Peason VII (Toraya, 1990) or pseudo-Voigt (Toraya, 1990); (iii) it allows outputs of the observed structure factors and their standard uncertainties, which are already corrected for anomalous scattering factors (Bagautdinov *et al.*, 1998) and Bijvoet pairs. These outputs are directly usable as input data for further MEM analysis if one wants to do so. The algorithm for simultaneous refinement for two data sets is described in the supplementary material.[1]

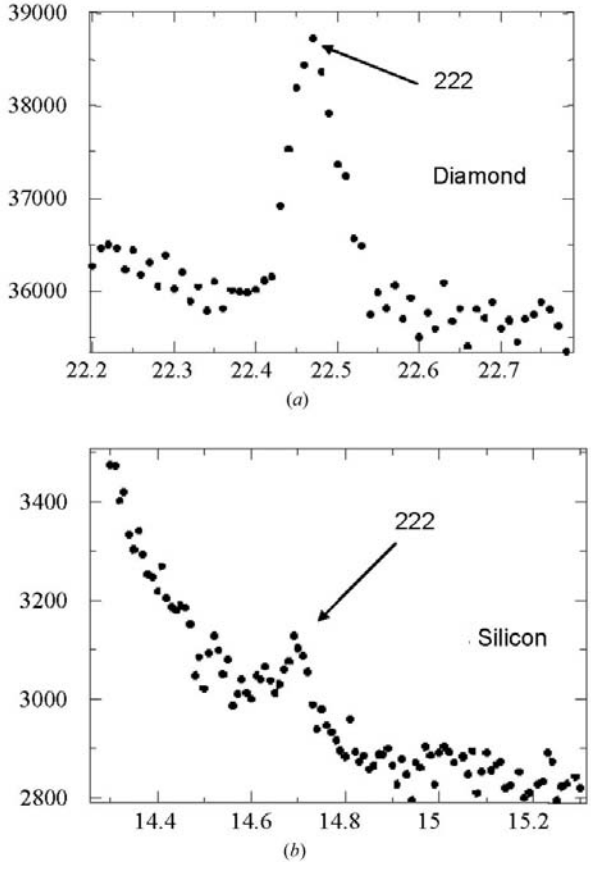

Figure 2
(*a*) Plot of the observed powder diffraction data for diamond 222 reflection. (*b*) Plot of the observed powder diffraction data for silicon 222 reflection.

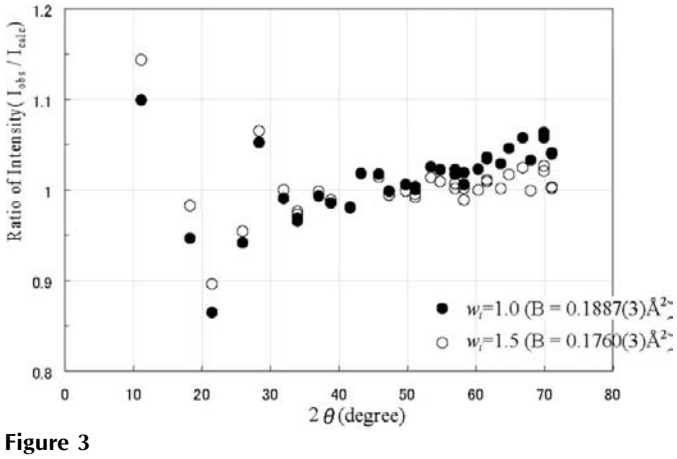

Figure 3
The plots of intensity ratios between observed intensities, I_{obs}, and calculated intensities, I_{cal}, for diamond data.

Intensity ratios, between observation and calculation, in the Rietveld refinement for diamond at 300 K are shown in Fig. 3. There are large plus and minus deviations in lower angular regions. It is well known that the reflections in lower angular regions include information on bonding electrons, since bonding electrons show broader distribution than core electrons. The deviations in the lower angular region must indicate the difference between the real electron-density distribution of a covalent atom and the electron-density distribution of a free atom. In the high-angle range, the ratio gradually increases with increasing diffraction angle. This indicates slight misestimation of thermal displacement parameters. It should be noted that the intensity of the 880 reflection, which locates at 79.99° in 2θ, is less than 0.2% of the intensity of the 111 reflection. The contribution to a reliability factor (R factor) of these weak intensities becomes negligibly small in the refinement if an ordinary weighting scheme, $w_i = Y_{oi}^{-1}$, is used. Because of this fact, it was not possible to refine thermal parameters any further. Toraya (1998) has proposed a new weighting scheme, *i.e.* $w_i = Y_{oi}^{-e}$ with $e \simeq 2$. This weighting scheme gives relatively heavier weights to weak reflections in Rietveld refinement. In order to determine the correct value of the thermal displacement parameter, we optimized the weight, w_i, based on the I_{obs}/I_{cal} plot. The intensity ratios between observation and calculation using the optimized weight value, $w_i = Y_{oi}^{-1.5}$, are shown by white circles in Fig. 3. The ratios in the high-angle region are distributed around 1.0 with a flat shape. This fact indicates the correct optimization of w_i.

The fitting results of Rietveld refinement using the above weighting scheme are shown in Figs. 4(*a*), (*b*) for silicon and Figs. 4(*c*), (*d*) for diamond. The R factors based on weighted profile, R_{wp}, and Bragg intensities, R_I, are listed in Table 1. The parameters determined by Rietveld refinement and other analytical conditions are also listed in the table. There are relatively larger uncertanties for three reflections at low angle, which must be the influence of covalent-bond electrons. In the higher-angle range, the deviations become very small. We determined the observed structure factors based on the Rietveld refinements. The details of intensity extraction are shown in the supplementary material.[1]

[1] Supplementary data for this paper, including two algorithms, structure factors and the numerical intensity of each measured point on the profile as a function of scattering angle for the Rietveld refinement, are available from the IUCr electronic archives (Reference: LB5005). Services for accessing these data are described at the back of the journal.

Table 1
Reliability factors and analytical conditions of silicon and diamond at 100 and 300 K.

	Temperature	Data range (2θ)		Resolution (Å)	Number of reflections	Weight w_i	R factors	
		D_1 (°)	D_2 (°)				R_{wp} (%)	R_I (R_B) (%)
Silicon	100 K	5–72	19–80	$d > 0.315$	133	1.5	3.88	1.55
	300 K	5–60	19–72	$d > 0.343$	105	1.6	2.70	1.75
Diamond	100 K	6–72	22–80	$d > 0.314$	42	1.5	2.73	3.92
	300 K	6–60	22–72	$d > 0.345$	37	1.5	2.93	3.74

4. Structure factors of silicon and diamond from powder diffraction data

The obtained structure factors of silicon and diamond are listed in Tables 2 and 3, respectively. The structure factors obtained from the *Pendellösung* method by Saka & Kato (1986) for silicon and for diamond by Takama *et al.* (1990) are also listed for reference. The experimental temperatures for Saka & Kato's and for Takama's data are 294 and 300 K, respectively. The structure factors in the $d > 0.48$ Å range are listed in Table 2. The structure factors in the $d > 0.63$ Å range are listed in Table 3. Though all of the reference data are listed in the tables, the number of data listed in the tables for the present study is less than 25% in each material. The full list of structure factors for the present studies have been deposited.[2] Comparison of the present silicon data at 300 K with Saka & Kato's data shows that the agreement between the two data sets is very good. The standard uncertainties in the present study have been estimated from counting statistics of the data. The standard uncertainties are from three to twenty times larger than those in Saka & Kato's data. The standard uncertainties in the $d < 1.0$ Å and $1.0 < d < 1.45$ Å ranges of the present data are approximately 1.0 and 5.4% of the values of the structure factors, respectively. The differences between the present data at 300 K and Saka & Kato's data are within standard uncertainties of the present structure-factor data. The present data at 300 K and Takama's data for diamond also show good agreement. The standard uncertainties in the present study are from one to five times larger than those in Takama's data. The standard uncertainties in the $d < 1.0$ Å and $1.0 < d < 1.45$ Å ranges of the present data are approximately 0.8 and 0.8%, respectively. The differences between the two data sets are within standard uncertainties of the present data. In order to evaluate the agreements between the present powder data and *Pendellösung* data, we calculated inter-data-set agreement factors, which are expressed as $\sum||F_{\rm powder}| - |F_{Pendellösung}||/\sum|F_{\rm powder}|$. This is 0.5% for silicon and 0.2% for diamond, respectively. Considering these values are obtained by totally different experimental methods, the agreement is excellent.

The theoretical structure factors of silicon and diamond have been extensively calculated. The structure factors are reported as atomic form factors, $f(hkl)$, which reveal the scattering factor of each atom in a crystal for a certain reflection (hkl). The conversion from atomic form factors to structure factors is very straightforward as long as the thermal parameters are known and *vice versa*. The form factors of silicon and diamond for the present powder data and theoretical calculation by Pere *et al.* (1999) are shown in Tables 4 and 5, respectively. The average difference between experi-

Table 2
Structure factors of silicon at 100 and 300 K determined from powder diffraction data (PDD).

Structure factors determined by the *Pendellösung* method (PM) are shown for reference (Saka & Kato, 1986).

$h\ k\ l$	PDD 100 K	PDD 300 K	PM 294 K
1 1 1	−60.4 (1)	−60.0 (1)	−60.13 (5)
2 2 0	−68.3 (1)	−67.2 (1)	−67.34 (5)
3 1 1	−44.3 (1)	−43.4 (1)	−43.63 (3)
2 2 2	1.6 (3)	1.6 (3)	
4 0 0	−57.7 (2)	−56.0 (2)	−56.23 (4)
3 3 1	39.7 (1)	38.5 (1)	38.22 (3)
4 2 2	51.3 (1)	49.3 (1)	49.11 (4)
3 3 3	34.5 (2)	32.9 (2)	32.83 (2)
5 1 1	34.5 (1)	32.9 (1)	32.94 (2)
4 4 0	45.5 (2)	43.1 (2)	42.88 (3)
5 3 1	30.7 (1)	28.9 (1)	28.81 (2)
6 2 0	40.3 (2)	37.4 (2)	37.59 (6)
5 3 3	−27.5 (2)	−25.5 (2)	−25.36 (4)
4 4 4	−36.5 (3)	−33.4 (3)	−33.18 (5)
5 5 1	−24.6 (2)	−22.5 (2)	−22.42 (3)
7 1 1	24.6 (2)	22.5 (2)	22.37 (3)
6 4 2	−32.7 (1)	−29.5 (1)	−29.42 (4)
7 3 1	−22.2 (1)	−19.9 (1)	−19.90 (3)
5 5 3	−22.2 (2)	−19.9 (2)	−19.98 (3)
8 0 0	29.1 (4)	25.8 (4)	26.23 (4)
7 3 3	−20.1 (2)	−17.6 (2)	−17.83 (3)
8 2 2	−26.9 (2)	−23.6 (3)	−23.48 (4)
6 6 0	−26.9 (3)	−23.6 (2)	−23.48 (4)
7 5 1	−18.4 (1)	−16.1 (2)	−15.98 (2)
5 5 5	18.3 (4)	16.0 (4)	15.98 (2)
8 4 0	−24.5 (2)	−21.4 (2)	−21.15 (3)
7 5 3	16.8 (2)	14.5 (2)	14.43 (2)
9 1 1	−16.8 (2)	−14.5 (2)	−14.46 (2)
6 6 4	22.8 (2)	19.4 (2)	19.13 (3)
9 3 1	−15.5 (2)	−13.1 (2)	
8 4 4	20.9 (2)	17.5 (3)	17.43 (12)
7 5 5	14.3 (2)	11.9 (3)	
7 7 1	14.3 (2)	11.9 (3)	
9 3 3	14.3 (2)	11.9 (3)	
8 6 2	19.2 (2)	16.0 (2)	
10 2 0	−19.2 (2)	−15.9 (3)	
9 5 1	13.4 (2)	11.0 (2)	
7 7 3	13.3 (2)	10.9 (3)	
9 5 3	12.4 (2)	9.9 (2)	
10 4 2	16.7 (2)	13.6 (2)	
7 7 5	−11.5 (3)	−9.1 (3)	
11 1 1	−11.5 (3)	−9.1 (3)	
8 8 0	16.2 (4)	12.8 (4)	12.41 (14)

[2] See deposition footnote 1.

mental and theoretical values is less than 1%. In order to evaluate the agreements between the present powder data and theoretical values, we again calculated an inter-data-set agreement factor expressed as $\sum||f_{\rm powder}| - |f_{\rm Theory}||/\sum|f_{\rm powder}|$. The values are within 0.53% for silicon and within 1.6% for diamond, as is shown in Tables 4 and 5.

5. Charge-density studies of silicon and diamond by MEM

The MEM analysis was carried out to investigate the usefulness of the present structure factors to reveal electron-density distributions. The program *ENIGMA* (Tanaka *et al.*, 2002) is used for MEM calculations. The unit cells of both silicon and diamond were divided into $128 \times 128 \times 128$ pixels. The reliability factors of the MEM analysis, $R_{\rm MEM}$, of silicon for 100 and 300 K data were both less than 1.0% and the $R_{\rm MEM}$ of diamond for 100 and 300 K data were both less than 0.6%. The contour maps of MEM charge densities for the (110) plane are shown in Fig. 5. The charge-density distributions indicating covalent bonds of silicon and diamond are very clearly shown in the figures.

The difference charge density, $\rho_{\rm diff}$, which corresponds to $\rho_{\rm 100K} - \rho_{\rm 300K}$, was calculated to visualize the thermal effect at the charge-density level. The $\rho_{\rm diff}$ of silicon is shown in Fig. 6(*a*). The positive and negative contour lines are shown as solid and dashed lines in the figure. In the core region, there are big differences, both positive and negative. The maximum difference of density in the core region is 170.731 e Å^{-3} at the peak position of the Si atom. This is obviously the effect of thermal vibrations of the nucleus. On the other hand, in the

Table 3
Structure factors of diamond at 100 and 300 K determined from powder diffraction data (PDD).

The structure factors determined by the *Pendellösung* method (PM) are shown for reference (Takama *et al.*, 1990).

h k l	PDD 100 K	PDD 300 K	PM 300 K
1 1 1	−18.07 (2)	−18.13 (2)	−18.37 (6)
2 2 0	−15.15 (3)	−15.13 (2)	−15.36 (5)
3 1 1	−9.06 (2)	−9.07 (2)	−9.32 (3)
2 2 2	1.1 (2)	1.0 (2)	
4 0 0	−11.78 (5)	−11.73 (5)	−11.93 (3)
3 3 1	8.31 (3)	8.30 (2)	8.39 (3)
4 2 2	10.66 (3)	10.61 (3)	10.9 (3)
5 1 1	7.14 (3)	7.12 (3)	7.41 (3)
3 3 3	7.13 (6)	7.09 (5)	7.28 (2)
4 4 0	9.63 (5)	9.56 (4)	9.58 (2)

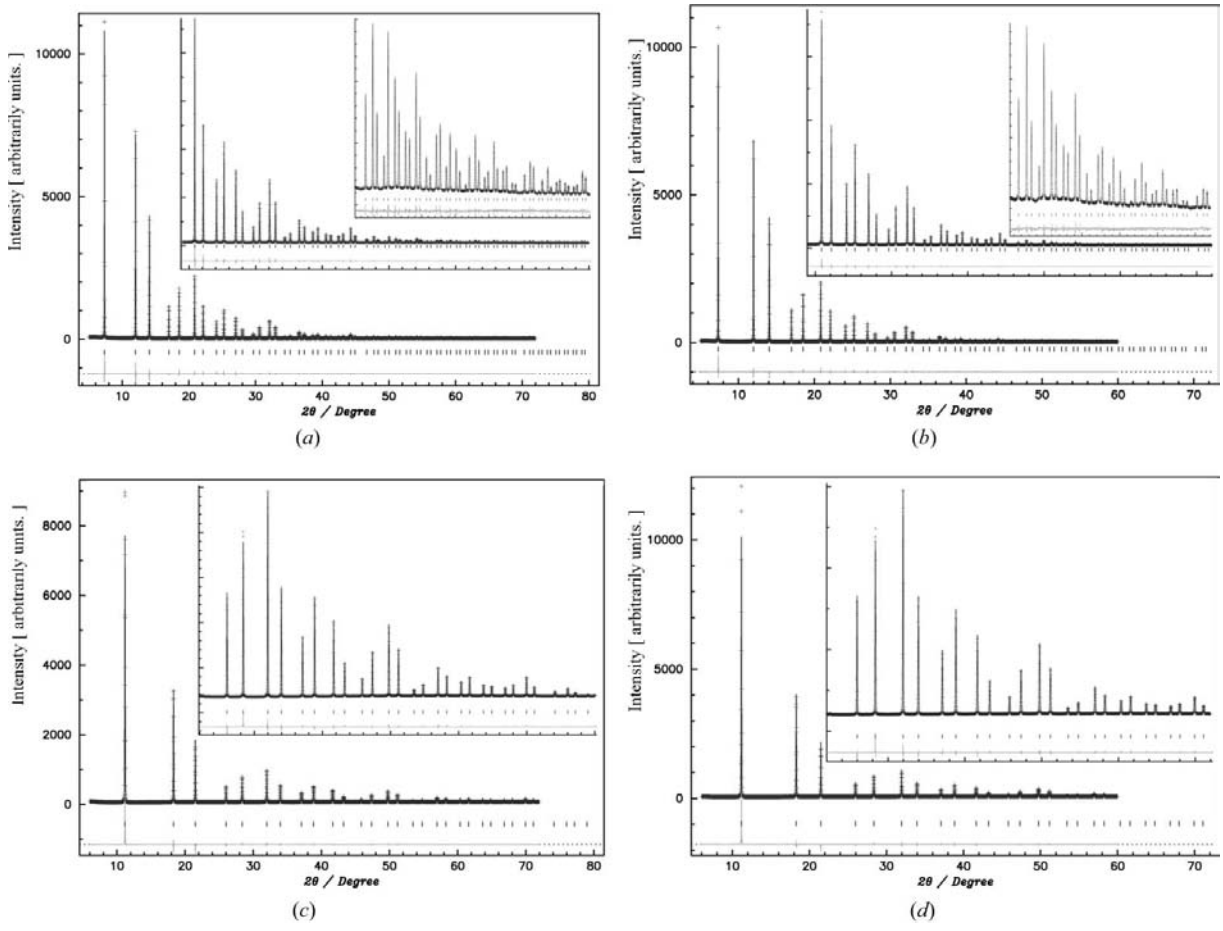

Figure 4
Fitting results of Rietveld refinement for silicon at (*a*) 100 K and (*b*) 300 K and diamond at (*c*) 100 K and (*d*) 300 K.

Table 4
Observed form factors for silicon at 300 K determined from powder diffraction data (PDD).

The form factors calculated by theoretical calculations at the HF, Lp and PW levels are shown for reference (Pere *et al.*, 1999). The thermal effects of observed form factors are removed by dividing by the thermal factors. The inter-data-set *R* factors between the powder data and the theoretical data are listed in the final line.

h k l	PDD	HF	Lp	PW
1 1 1	10.73 (1)	10.742	10.720	10.727
2 2 0	8.65 (1)	8.651	8.663	8.659
3 1 1	8.00 (2)	8.012	8.036	8.031
2 2 2	0.22 (4)	0.203	0.135	0.151
4 0 0	7.43 (3)	7.460	7.440	7.448
3 3 1	7.31 (2)	7.268	7.205	7.222
4 2 2	6.74 (2)	6.725	6.686	6.698
3 3 3	6.43 (4)	6.459	6.423	6.435
5 1 1	6.44 (2)	6.415	6.398	6.406
4 4 0	6.07 (3)	6.060	6.025	6.036
5 3 1	5.83 (2)	5.822	5.793	5.803
6 2 0	5.44 (2)	5.477	5.450	5.459
5 3 3	5.29 (4)	5.290	5.261	5.270
4 4 4	5.01 (5)	4.983	4.959	4.966
5 5 1	4.82 (4)	4.818	4.795	4.802
7 1 1	4.82 (4)	4.813	4.792	4.799
6 4 2	4.55 (2)	4.556	4.536	4.543
5 5 3	4.39 (4)	4.413	4.395	4.400
7 3 1	4.39 (5)	4.412	4.393	4.399
8 0 0	4.11 (6)	4.188	4.172	4.177
7 3 3	4.01 (5)	4.064	4.047	4.053
6 6 0	3.87 (5)	3.871	3.856	3.861
8 2 2	3.87 (4)	3.871	3.856	3.861
5 5 5	3.75 (9)	3.762	3.748	3.752
7 5 1	3.78 (4)	3.761	3.749	3.753
8 4 0	3.61 (4)	3.596	3.583	3.587
7 5 3	3.51 (4)	3.504	3.492	3.495
9 1 1	3.50 (5)	3.501	3.490	3.494
6 6 4	3.38 (4)	3.356	3.345	3.349
8 4 4	3.14 (4)	3.147	3.138	3.141
8 8 0	2.59 (8)	2.537	2.531	2.533
R (%)		0.37	0.57	0.49

Table 5
Observed form factors of diamond for 300 K determined from powder diffraction data (PDD).

The form factors calculated by theoretical calculations at the HF, Lp and PW levels are shown for reference (Pere *et al.*, 1999). The thermal effects of observed form factors are removed by dividing by the thermal factors. The inter-data-set *R* factors between the powder data and the theoretical data are listed in the final line.

h k l	PDD	HF	Lp	PW
1 1 1	3.238 (3)	3.287	3.294	3.299
2 2 0	1.943 (3)	1.940	1.967	1.967
3 1 1	1.664 (3)	1.667	1.700	1.699
2 2 2	0.13 (3)	0.131	0.100	0.103
4 0 0	1.548 (6)	1.568	1.558	1.560
3 3 1	1.566 (4)	1.560	1.569	1.570
4 2 2	1.439 (3)	1.444	1.441	1.443
5 1 1	1.381 (5)	1.396	1.392	1.394
3 3 3	1.375 (10)	1.373	1.376	1.377
4 4 0	1.334 (7)	1.329	1.324	1.326
5 3 1	1.287 (5)	1.283	1.279	1.282
6 2 0	1.220 (5)	1.224	1.218	1.221
5 3 3	1.209 (8)	1.195	1.187	1.191
4 4 4	1.149 (9)	1.133	1.127	1.130
7 1 1	1.109 (8)	1.103	1.097	1.100
5 5 1	1.109 (8)	1.100	1.094	1.098
6 4 2	1.067 (5)	1.051	1.045	1.049
5 5 3	1.032 (9)	1.023	1.017	1.021
7 3 1	1.036 (6)	1.020	1.015	1.018
8 0 0	0.998 (10)	0.977	0.971	0.975
7 3 3	0.973 (10)	0.950	0.945	0.949
6 6 0	0.923 (10)	0.910	0.905	0.909
8 2 2	0.927 (8)	0.910	0.905	0.910
7 5 1	0.904 (8)	0.889	0.883	0.887
5 5 5	0.89 (1)	0.887	0.882	0.886
8 4 0	0.866 (8)	0.850	0.845	0.849
7 5 3	0.848 (8)	0.830	0.825	0.829
9 1 1	0.848 (12)	0.829	0.824	0.827
6 6 4	0.810 (9)	0.796	0.791	0.795
8 4 4	0.769 (10)	0.746	0.742	0.745
R (%)		1.09	1.44	1.41

bond region, there are almost no differences in the figure. The level of difference is less than 0.05 e Å^{-3}.

The $\rho_{\rm diff}$ of diamond are shown in Fig. 6(*b*). There are also both positive and negative differences in the core region. The maximum difference in the core region is 10.764 e Å^{-3} at the peak position of the C atom. In the bond region, there are small negative charge-density regions from −0.15 to −0.05 e Å^{-3}. The difference is less than 0.15 e Å^{-3}. The $\rho_{\rm diff}$ of both silicon and diamond demonstrates that the charge density in the bond regions is not greatly affected by the temperature variation. The temperature mainly affects electrons in the core region. This fact suggests that the experimental charge densities in the bonding regions observed at finite temperature would still be comparable to the theoretical calculations at least for the present two materials. There would be many other materials for which the above statement is valid.

The charge densities by theoretical calculation for silicon and diamond have been widely reported by many researchers. Most of the charge densities are reported as a valence map without thermal motion effects (Yin & Cohen, 1982; Van Camp & Devreese, 1986; Fukumoto, 1990; Zandiehnadem & Ching, 1990; Lu *et al.*, 1993). In order to compare the present MEM densities with other theoretical valence maps in detail, we have calculated valence charge density from MEM charge density expressed as $\rho_{\rm val} = \rho_{\rm all} - \rho_{\rm core}$. The $\rho_{\rm all}$ are the MEM charge densities at 100 K shown in Figs. 5(*a*), (*c*). The $\rho_{\rm core}$ are calculated by the following procedures. We used the form factor of core electrons for silicon and diamond listed in *International Tables for X-ray crystallography* (1964). The structure factors of core electrons, $F_{\rm core}(hkl)$, were calculated by multiplication of $8\cos[0.25\pi(h+k+l)]$ and thermal displacement factors to form factors. The $\rho_{\rm core}$ were calculated by MEM using $F_{\rm core}(hkl)$ and $\sigma(hkl)$. The $\sigma(hkl)$ of the present silicon and diamond powder data were also used in the $\rho_{\rm core}$ calculations.

The density maps of $\rho_{\rm val}$ for silicon and diamond calculated by the above processes are shown in Figs. 7(*a*), (*b*). The charge density at the bond midpoint for silicon and diamond are 0.56 and 1.64 e Å^{-3}, respectively. The theoretical value of the valence densities for silicon are 0.55 (Fukumoto, 1990) and 0.56 e Å^{-3} (Lu *et al.*, 1993) and that for diamond are 1.65 (Fukumoto, 1990) and 1.59 e Å^{-3} (Lu *et al.*, 1993). The values

of the present study are identical to those of theoretical calculations within 0.05 e Å^{-3}. These show that present MEM charge densities are quantitatively reliable and can be used to discuss the physical properties of materials.

6. Advantages of present high-resolution powder data in charge-density studies

The MEM charge density of silicon at 294 K had previously been calculated using Saka & Kato's *Pendellösung* data (Takata & Sakata, 1996). We compared the MEM charge density of the previous study with that of the present study for an evaluation of the accuracy in charge density. The features of the previous charge density are very similar to Fig. 5(*b*). The slight difference is found at the bond mid-point. There is a small charge-density peak at the bond mid-point in the previous charge density (Takata & Sakata, 1996), which is called the non-nuclear maximum (Jauch & Palmer, 1993; de Vries *et al.*, 1996). On the other hand, no such peak is found in Fig. 5(*b*). Such non-nuclear maxima appear even if we use the present powder data where the number of data is limited as in the case of Takata & Sakata (1996). Therefore, it can be concluded that a low number of structure-factor data causes the non-nuclear maxima in the Si—Si covalent bond.

In order to study the resolution effects in the MEM charge-density distribution, one-dimensional charge densities along the [111] direction of the previous and the present studies are shown in Fig. 8. The charge densities around the atomic position are shown in the figure. The maximum charge-density value at an atomic position of the previous study is 204.9 e Å^{-3}, which is much lower than that of the present study, *i.e.* 267.4 e Å^{-3}. We carried out least-squares fitting of a Gaussian function to the charge-density profiles of Fig. 8. The full width at half-maximum (FWHM) of the previous charge density is 0.317 Å. The FWHM of the present charge density is 0.272 Å. This is because the lack of resolution causes smearing of the sharp charge-density distribution. The *d*-spacing range of Saka & Kato's data is $d > 0.58$ Å, which is much smaller than that of the present data, $d > 0.343$ Å. To confirm resolution effects, we carried out MEM analysis by using $d > 0.58$ Å structure factors of the present study. The charge-density peak at the atomic position is decreased to 205.87 e Å^{-3}. This analysis confirms the above-mentioned resolution effects in the MEM charge density. From the

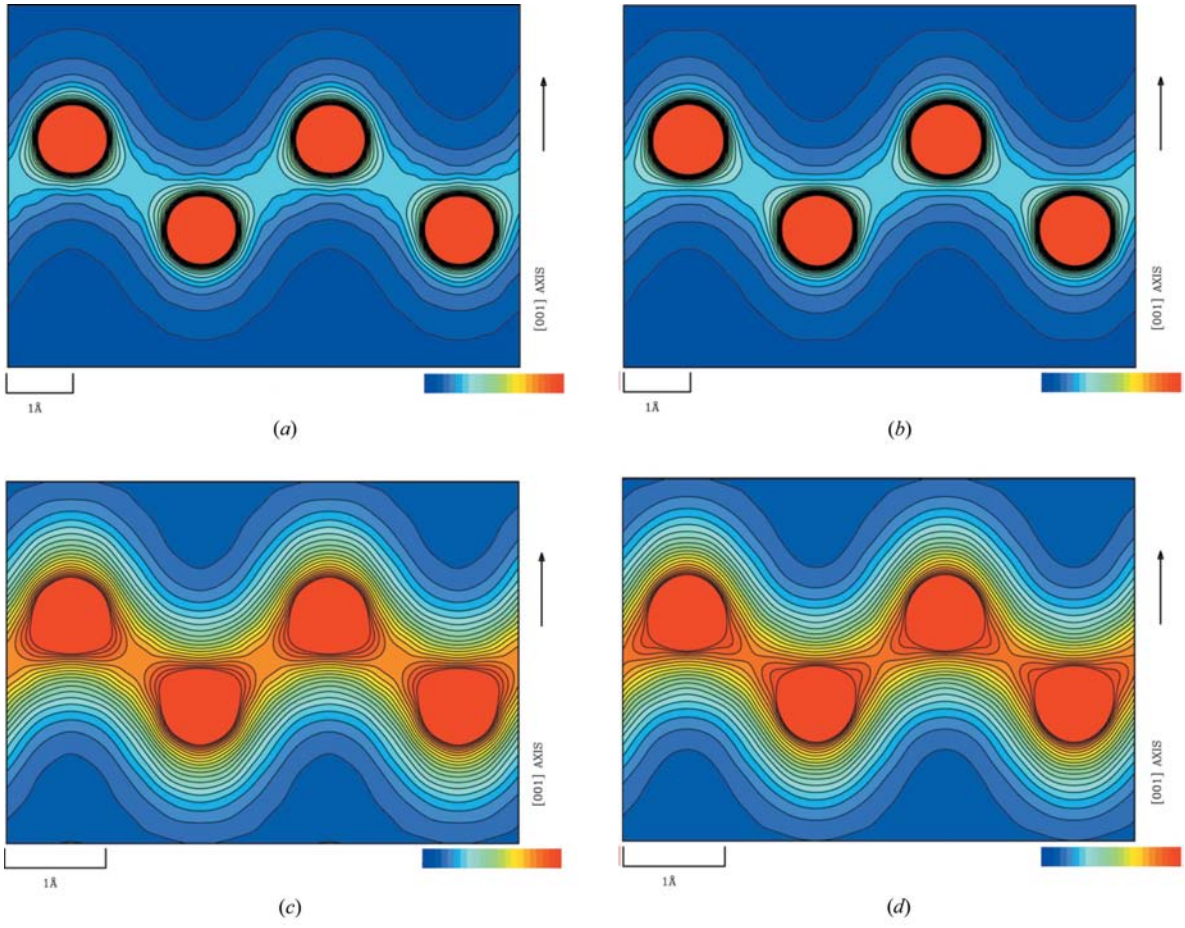

Figure 5
(*a*) The MEM charge density of silicon at 100 K, ρ_{100K}, determined by the present study. (*b*) The MEM charge density of silicon at 300 K, ρ_{300K}. (*c*) The MEM charge density of diamond at 100 K, ρ_{100K}, determined by the present study. (*d*) The MEM charge density of diamond at 300 K, ρ_{300K}. The contour lines are drawn from 0.1 to 2.0 e Å^{-3} with 0.1 e Å^{-3} step width for (*a*), (*b*), (*c*) and (*d*).

comparison of the MEM analyses between Saka & Kato's data and of the present powder data, it may be said that accurate powder data of a wide *d*-spacing range are more appropriate for a MEM charge-density study.

7. Concluding remarks

In this study, we measured accurate structure factors of silicon and diamond with a synchrotron X-ray powder diffraction experiment. We evaluated the accuracy of the structure factors by comparison with the *Pendellösung* data and theoretical calculations. These results show that powder diffraction data measured at SPring-8 BL02B2 are highly reliable. We also showed the usefulness of the structure factors in a MEM charge-density study. It is also shown that the present data are most appropriate for an experimental charge-density study of silicon and diamond. Since the data have enough accuracy, the present method can be widely applicable for various materials in powder form.

We also report both experimental and analytical techniques for extraction of accurate structure factors from powder diffraction data. The powder data for a charge-density study require homogeneous intensity distribution of Debye–Scherrer ring and sufficient counting statistics. The methods, sample preparation, multi-data measurement, simultaneous multi-data refinement and weight adjustment, described here, can improve the qualities of advanced structural studies by powder specimens. Each method is easy to apply to other materials. The accurate charge density of functional materials, such as superconductors, can be performed by the present method. Present results suggest that powder diffraction by a third-generation synchrotron X-ray source is a promising

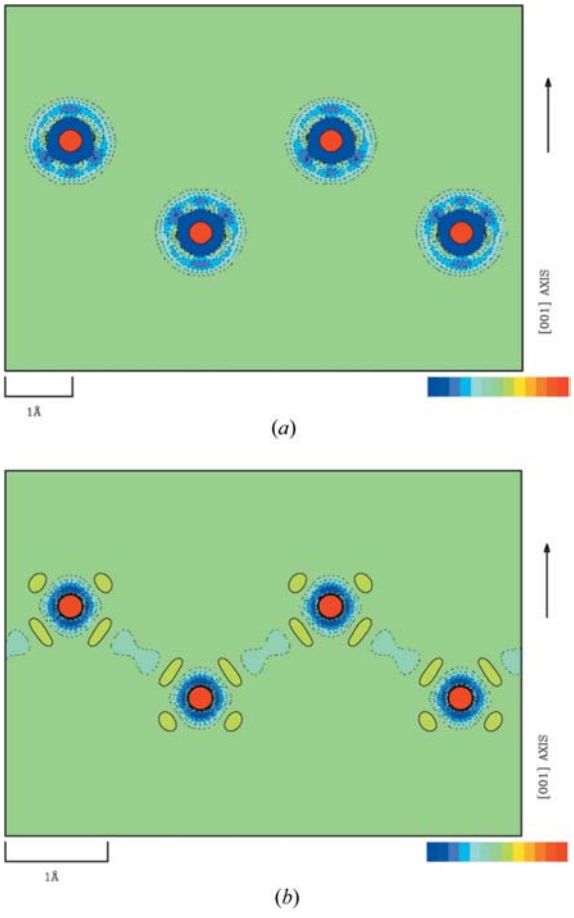

Figure 6
(*a*) The difference of MEM charge densities, $\rho_{\rm diff}$, for silicon expressed as $\rho_{100\rm K} - \rho_{300\rm K}$. (*b*) The difference of MEM charge densities, $\rho_{\rm diff}$, for diamond expressed as $\rho_{100\rm K} - \rho_{300\rm K}$. The contour lines are drawn from -0.55 to 0.55 e Å^{-3} with 0.1 e Å^{-3} step width for (*a*) and (*b*).

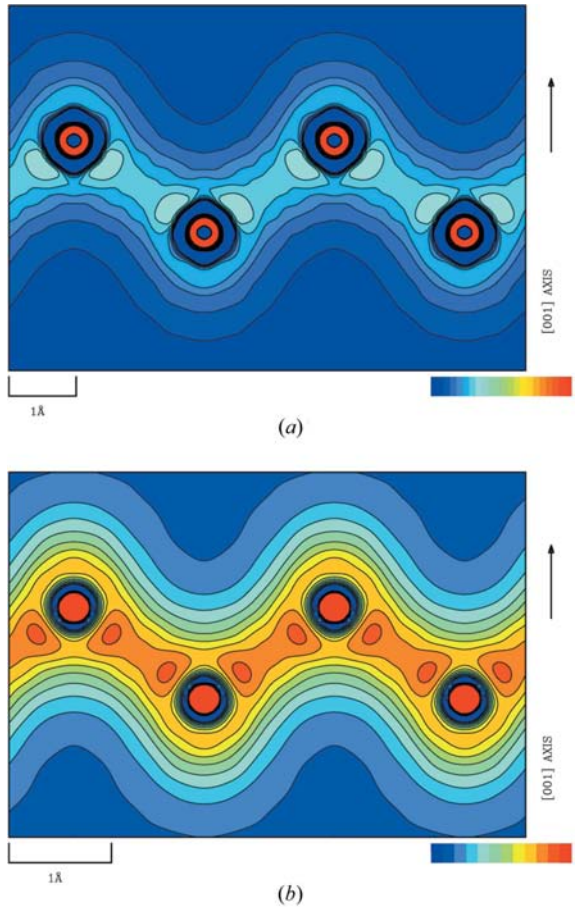

Figure 7
The valence charge densities of (*a*) silicon and (*b*) diamond based on MEM analysis.

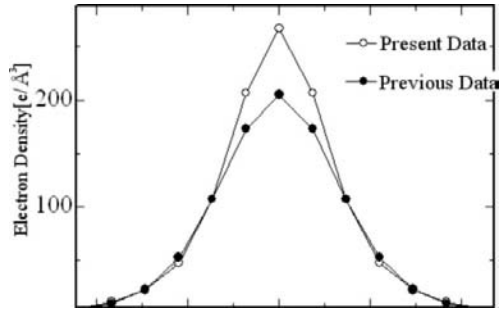

Figure 8
One-dimensional MEM charge densities of silicon based on the present powder data and the previous *Pendellösung* data.

method to reveal accurate charge density in the materials science fields.

The authors thank H. Tanaka for development of the MEM charge-density program *ENIGMA*. This work has been supported by the JST CREST Programme, the Grant-Aid for Young Scientists A (No. 17686003) of Mext, and Toyota Riken Foundation. The synchrotron-radiation experiments were performed at beamline BL02B2 at SPring-8 with the approval of the Japan Synchrotron Radiation Research Institute (JASRI).

References

Amemiya, Y. (1995). *J. Synchrotron Rad.* **2**, 13–21.
Bagautdinov, B., Luedecke, J., Schneider, M. & van Smaalen, S. (1998). *Acta Cryst.* B**54**, 626–634.
Fukumoto, A. (1990). *Phys. Rev. B*, **42**, 7462–7469.
Hammersley, A. P., Svensson, S. O., Hanfland, M., Fitch, A. N. & Häusermann, D. (1996). *High Press. Res.* **14**, 235–248.
International Tables for X-ray Crystallography (1964). Vol. IV. Birmingham: Kynoch Press.
Jauch, W. & Palmer, A. (1993). *Acta Cryst.* A**49**, 590–591.
Kuroiwa, Y., Aoyagi, S., Sawada, A., Harada, J., Nishibori, E., Takata, M. & Sakata, M. (2001). *Phys. Rev. Lett.* **87**, 217601.
Larson, A. C. & von Dreele, R. B. (1990). *General Structure Analysis System* (*GSAS*), Los Alamos National Laboratories, NM, USA.
Lu, Z. W., Zunger, A. & Moshe, D. (1993). *Phys. Rev. B*, **47**, 9385–9410.
Nishibori, E., Takata, M., Kato, K., Sakata, M., Kubota, Y., Aoyagi, S., Kuroiwa, Y., Yamakata, M. & Ikeda, N. (2001). *Nucl. Instrum. Methods*, A**467**, 1045–1048.
Nishibori, E., Takata, M., Sakata, M., Tanaka, H., Muranaka, T. & Akimitsu, J. (2001). *J. Phys. Soc. Jpn*, **70**, 2252–2254.
Nishibori, E., Takata, M., Sakata, M., Taninaka, A. & Shinohara, H. (2001). *Angew. Chem. Int. Ed. Engl.* **40**, 2998–2999.
Pere, J., Duvignau, G.-D. & Lichanot, A. (1999). *J. Phys. Condens. Matter*, **11**, 5827–5843.
Roisnel, T. & Rodriguez-Carvajal, J. (2001). *Mater. Sci. Forum*, **118**, 378–381.
Saka, T. & Kato, N. (1986). *Acta Cryst.* A**42**, 469–477.
Sakata, M. & Sato, M. (1990). *Acta Cryst.* A**46**, 263–270.
Spackman, M. A. (1986). *Acta Cryst.* A**42**, 271–281.
Spackman, M. A. (1991). *Acta Cryst.* A**47**, 420–427.
Takama, T., Tsuchiya, K., Kobayashi, K. & Sato, S. (1990). *Acta Cryst.* A**46**, 514–517.
Takata, M. & Sakata, M. (1996). *Acta Cryst.* A**52**, 287–290.
Tanaka, H., Takata, M., Nishibori, E., Kato, K., Iishi, T. & Sakata, M. (2002). *J. Appl. Cryst.* **35**, 282–286.
Teworte, R. & Bonse, U. (1984). *Phys. Rev. B*, **29**, 2102–2108.
Toraya, H. (1990). *J. Appl. Cryst.* **23**, 485–491.
Toraya, H. (1998). *J. Appl. Cryst.* **31**, 333–343.
Trail, J. R. & Bird, D. M. (1999). *Phys. Rev. B*, **60**, 7875–7880.
Van Camp, P. E. & Devreese, J. T. (1986). *Phys. Rev. B*, **34**, 1314–1316.
Vries, R. Y. de, Briels, W. J. & Feil, D. (1996). *Phys. Rev. Lett.* **77**, 1719–1722.
Yin, M. T. & Cohen, M. L. (1982). *Phys. Rev. B*, **26**, 5668–5687.
Zandiehnadem, F. & Ching, W. Y. (1990). *Phys. Rev. B*, **41**, 12162–12179.
Zuo, J. M., Blaha, P. & Schwarz, K. (1997). *J. Phys. Condens. Matter*, **9**, 7541–7561.